AMERICAN ACADEMY OF OPHTHALMOLOGY®

# Severity Scale of Diabetic Macular Ischemia Based on the Distribution of Capillary Nonperfusion in OCT Angiography

*Miyo Yoshida, MD, Tomoaki Murakami, MD, PhD, Keiichi Nishikawa, MD, Kenji Ishihara, MD, PhD, Yuki Mori, MD, PhD, Akitaka Tsujikawa, MD, PhD*

***Purpose:*** To evaluate the severity scales of diabetic macular ischemia (DMI) by analyzing the quantity and distribution of capillary nonperfusion using OCT angiography (OCTA) images.

***Design:*** A single-center, prospective case series.

***Participants:*** Three hundred one eyes from 301 patients with diabetic retinopathy.

***Methods:*** We acquired 3 × 3-mm swept-source OCTA images and created en face images within a central 2.5-mm circle. The circle was divided into 15 × 15-pixel squares and nonperfusion squares (NPSs) were defined as those without retinal vessels. Eyes with high-dimensional spatial data were arranged on a 2-dimensional space using the uniform manifold approximation and projection (UMAP) algorithm and classified by clustering into 5 groups: *Initial*, *Mild*, *Superficial*, *Moderate*, and *Severe*.

***Main Outcome Measures:*** Development of a severity scale for DMI.

***Results:*** Eyes arranged on a 2-dimensional UMAP space were divided into 5 clusters, based on the similarity of nonperfusion area distribution. Nonperfusion square counts in the deep layer increased in eyes of the *Initial*, *Mild*, *Moderate*, and *Severe* groups in a stepwise manner. In contrast, there were no significant changes in superficial NPS counts between eyes of the *Initial* and *Mild* groups. In the intermediate stage, eyes of the *Superficial* group exhibited higher NPS counts in the central sector of the superficial layer compared with those of the *Moderate* group. The foveal avascular zone extended into the temporal subfield of the deep layer in eyes of the *Moderate* group. Eyes of the *Severe* group had significantly poorer visual acuity that was more frequently accompanied with proliferative diabetic retinopathy.

***Conclusions:*** The application of dimensionality reduction and clustering has facilitated the development of a novel severity scale for DMI based on the distribution of capillary nonperfusion in OCTA images.

***Financial Disclosure(s):*** The authors have no proprietary or commercial interest in any materials discussed in this article. 

*Supplemental material available at www.ophthalmologyscience.org.*

Capillary nonperfusion is a hallmark of progressive pathogenesis in diabetic retinopathy (DR).[1] In the macula, diabetic macular ischemia (DMI) often leads to visual impairment, including visual acuity (VA) reduction and poor sensitivity.[2–6] Despite its clinical significance, the progression characteristics of DMI remain inadequately understood, with diagnostic criteria and severity grading yet to be fully established.[7,8]

Enhanced visualization of the different retinal vascular plexuses using OCT angiography (OCTA) has renewed interest in understanding DMI better.[9–11] Previously, fluorescein angiography (FA) was the gold standard for DMI assessment, focusing on morphologic parameters in the foveal avascular zone (FAZ) as the primary biomarkers for grading DMI.[12] OCT angiography surpasses FA by offering detailed insights into the parafoveal capillaries and the deep capillary plexuses, whose loss correlates significantly with visual impairment.[3,4,13–17] Spatiotemporal characteristics of macular capillary nonperfusion and their clinical implications remain to be elucidated to propose a novel approach to grade DMI severity.

Dimensionality reduction techniques, essential for transforming complex, high-dimensional data sets into more manageable, lower-dimensional representations, play a crucial role in data visualization and preprocessing of data analyses.[18] Among these techniques, uniform manifold approximation and projection (UMAP) stands out for its scalability and versatility across various data types.[19] Its strength lies in its capacity for feature extraction and visualization, enabling 2-dimensional displays that facilitate data clustering. This methodology has recently been applied to delineate clinical characteristics from multidimensional data, leading to implications for disease grading.[20,21]



https://doi.org/10.1016/j.xops.2024.100603
ISSN 2666-9145/24

In this study, we aim to investigate an objective severity scale of DMI in high-dimensional OCTA images utilizing UMAP and subsequent clustering.

## Methods

### Participants

This prospective study enrolled patients with DR examined at the Department of Ophthalmology in Kyoto University Hospital. This study was conducted under the approval of the Kyoto University Graduate School and Faculty of Medicine Ethics Committee and in adherence to the tenets of the Declaration of Helsinki. All participants provided written informed consent before inclusion in the study.

We assessed eyes with DR for which swept-source OCTA (SS-OCTA) images of sufficient quality (signal strength index of 8 or more) were obtained. The inclusion criteria were the presence of DR, the acquisition of central 3 × 3-mm SS-OCTA images centered on the fovea, and written informed consent. Exclusion criteria were severe media opacity, an axial length of <22 mm or >26 mm, any other chorioretinal disease including glaucoma, epiretinal membrane, and vitreomacular traction, other ocular diseases that lead to visual impairment, or previous treatment within 6 months before imaging such as intraocular surgery, anti-VEGF injection, ocular steroids, and photocoagulation. Additional exclusion criteria were poor image quality (signal strength index of ≤7) or severe segmentation error in the superficial slab. If both eyes met the inclusion criteria, we selected the right eye for this study.

### Image Acquisition and Processing

Best-corrected decimal VA was measured and converted to the logarithm of the minimum angle of resolution (logMAR) VA. Comprehensive ophthalmic examinations were conducted, including severity assessment of DR based on the International Clinical Diabetic Retinopathy Severity Scales.[22] Axial length and central subfield thickness (CST) were measured using partial coherence interferometry (IOL Master, Carl Zeiss Meditec, Inc) and Spectralis OCT (Heidelberg Engineering), respectively. Eyes with a CST of >320 μm or 305 μm for male or female patients, respectively, were diagnosed as center-involved diabetic macular edema (DME).[23]

Swept-source OCTA images within the nominal 3 × 3-mm square centering on the fovea were acquired using Plex Elite 9000 (Carl Zeiss Meditec, Inc). The images of the left eye were inverted horizontally to standardize the nasal subfield positioning. The nominal 3 × 3-mm square was obtained with 300 × 300 A-scans and digitally converted to a 1024 × 1024-pixel array for quantitative analyses. For the superficial layer, default setting from the inner limited membrane to the boundary of the inner plexiform layer and inner nuclear layer was used. To avoid segmentation errors in DME eyes and artifacts from various sources, another slab image from the inner border of the inner nuclear layer to 70 μm above the retinal pigment epithelium was utilized, employing the custom setting of the same software, as mentioned earlier.[24]

We employed a semiautomatic procedure to determine the amounts and locations of nonperfusion areas (NPAs) on SS-OCTA images. This involved stepwise image processing: (1) adjustment of image brightness; (2) determination of the foveal center; (3) automatic detection of NPAs; and (4) assessment of NPA amounts and locations. After the automatic adjustment of brightness and contrast in the en face deep layer images (enhance contrast, saturated = 0.35), the circle with a diameter of 2.5 mm centering the foveal center was determined. The edges of retinal vessels were automatically traced using edge detection, utilizing the Canny Edge Detector plugin of ImageJ software (default setting; National Institutes of Health, http://imagej.nih.gov/ij/).[25] The circle was divided into 15 × 15-pixel squares, resulting in a total of 5004 squares in both superficial and deep layers. The squares without any signals of vascular edges were defined as nonperfusion squares (NPSs) in this study (Fig 1). Each eye was encoded as a single 5004-dimensional binary vector that combines data from both the superficial and deep layers, enabling a comprehensive analysis of the retinal vasculature.

To explore the distribution of capillary nonperfusion, we counted the NPSs in 5 subfields of the ETDRS grid (a central 1-mm area and 4 parafoveal sectors [1−2.5 mm]). As another approach, we defined the NPS ratio for each square as follows.[26]

Vessel density (VD) was calculated for comparison with NPS from binarized images generated using the Phansalkar adaptive local thresholding method of ImageJ (white and black pixels representing blood vessels and background, respectively). White pixels were quantified and divided by the number of total pixels to calculate the VD as described previously.[27] The FAZ areas were measured as previously described.[17] Briefly, the "Analyze Particles" function in ImageJ was applied to binarized images to automatically determine intercapillary spaces. In this study, we defined the space containing the foveal center as the FAZ.

## Dimensionality Reduction and Clustering

We utilized UMAP for nonlinear dimensionality reduction, as described previously.[20] The Euclidean distance for 3 neighbors with a minimum distance of 0.1 was used to develop the manifold. All other parameters remained at the default values reported by McInnes et al.[19] After the NPSs in both superficial and deep layers were integrated, each eye with 5004-dimensional data was mapped onto a 2-dimensional space reflecting the similarity of the NPSs distribution. To identify the optimal number of clusters, we employed the elbow method and determined the cluster number based on nonperfusion metrics such as NPS counts and FAZ size, as well as perfusion metrics like VD. We then performed clustering using the *k*-means algorithm.

Objective clustering organized 301 eyes into 5 clusters. These clusters were categorized based on the quantity and distribution of the NPSs as *Initial*, *Mild*, *Superficial*, *Moderate*, and *Severe*, respectively. The *Initial* group consisted of eyes with minimal NPSs in both the superficial and deep layers. Eyes of the *Mild* group displayed minimal NPSs in the superficial layer but more NPSs in the deep layer. Eyes with the highest NPSs across both layers were classified as the *Severe* group. In the intermediate classification, eyes with an increased number of NPSs in the central sector of the superficial layer were designated as those of the *Superficial* group, whereas eyes with more NPSs in the temporal sector of the deep layer were categorized as the *Moderate* group.

### Statistical Analyses

All values were expressed as the median (interquartile range). Statistical significance was set at $P < 0.05$. After verifying normal distribution with Shapiro−Wilk test, we used the Kruskal−Wallis test with a Bonferroni correction for continuous variables and the chi-square test for categorical variables. The statistical associations were evaluated

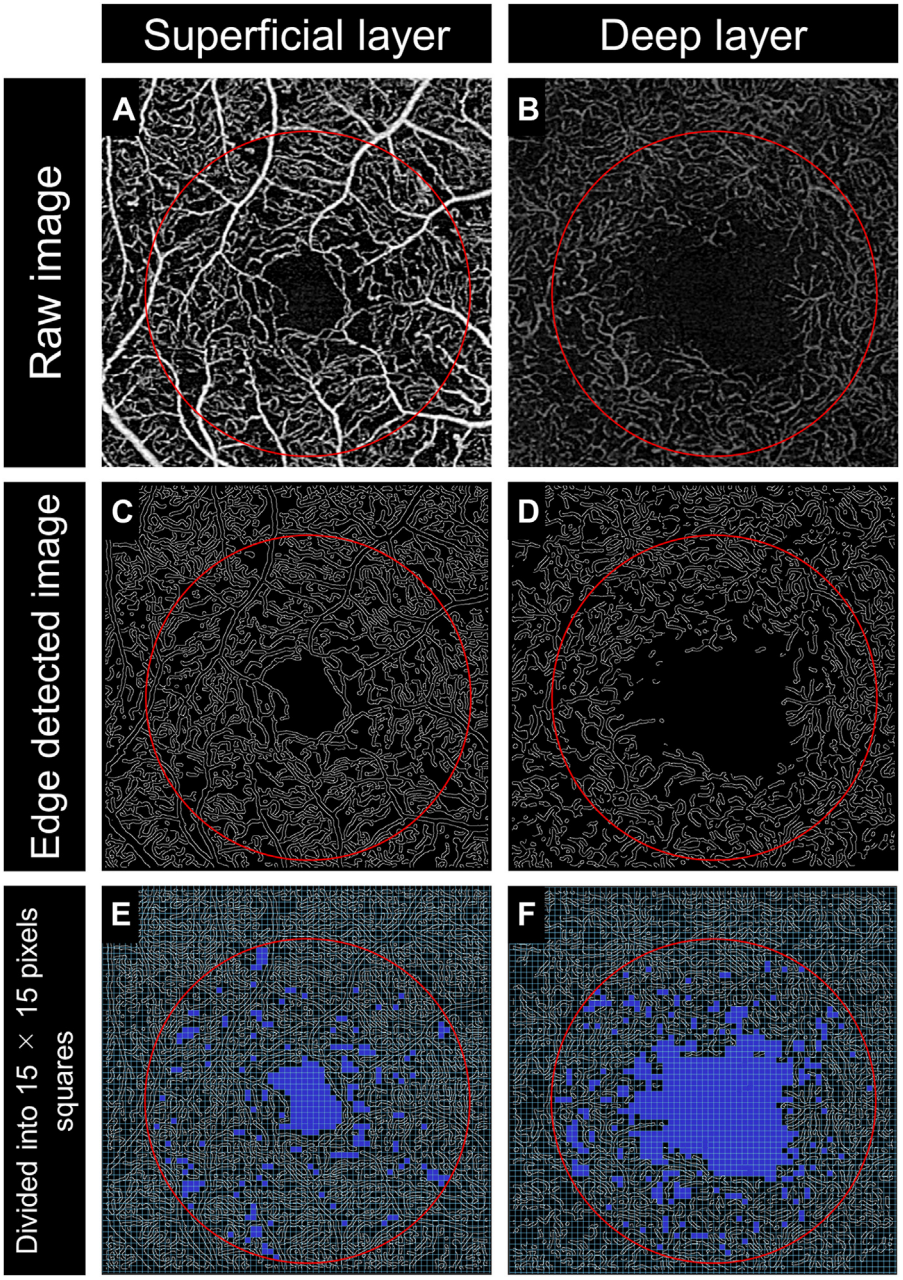


**Figure 1.** Semiautomatic assessment of nonperfusion areas on en face OCT angiography (OCTA) images in a 54-year-old representative case with proliferative diabetic retinopathy. The superficial layer using the default setting of the manufacturer's software (**A, C, E**) and in the deep en face OCTA images with the custom setting (from the inner nuclear layer to the outer nuclear layer) (**B, D, F**). **A, B,** Raw images. **C, D,** The binary images using the edge detection function of the ImageJ software plugin. **E, F,** The binary images are divided into squares of 15 × 15 pixels, with nonperfusion squares highlighted in blue.

using Spearman's rank correlation coefficient. All statistical analyses were conducted using SPSS (version 24; IBM).

## Results

In this cross-sectional study, we analyzed 301 eyes from 301 patients with DR, with their characteristics displayed in Table 1. The NPS counts, automatically determined through image processing, were compared with the VD (Fig S2, available at www.ophthalmologyscience.org). There were significant negative correlations between these parameters in all 301 eyes across both superficial and deep layers (Fig S2A, B). The correlation was notably stronger in eyes without DME (Fig S2C, D) and less pronounced in those with DME (Fig S2E, F).

The UMAP algorithm mapped the 301 eyes onto a 2-dimensional space reflecting the NPS distribution

Table 1. Patients' Characteristics

| Variables | |
|---|---|
| Eyes/patients | 301/301 |
| Age (yrs) | 64 (53–71) |
| Sex (male/female) | 196/105 |
| Hemoglobin A1c (%) | 7.3 (6.7–8.5) |
| Duration of diabetes (yrs) | 16 (10–22) |
| Systemic hypertension (present/absent) | 179/122 |
| Dyslipidemia (present/absent) | 124/177 |
| logMAR VA | 0.000 (−0.079 to 0.155) |
| Phakia/pseudophakia | 170/131 |
| International DR severity grade (eyes) | |
| Mild NPDR | 18 |
| Moderate NPDR | 139 |
| Severe NPDR | 31 |
| PDR | 113 |
| Diabetic macular edema (present/absent) | 106/195 |
| Central subfield thickness (μm) | 290 (267–339) |
| Prior PRP (present/absent) | 124/177 |
| Prior STTA (present/absent) | 25/276 |
| Prior anti-VEGF injection (present/absent) | 39/262 |
| Prior vitrectomy (present/absent) | 35/266 |
| NPS counts in the superficial layer | 279 (196–382) |
| NPS counts in the deep layer | 759 (581–1017) |
| NPS counts in both layers | 1036 (802–1382) |
| VD in the superficial layer (%) | 36.3 (31.3–41.4) |
| VD in the deep layer (%) | 18.8 (14.1–24.2) |

DR = diabetic retinopathy; logMAR VA = logarithm of the minimum angle of resolution visual acuity; NPDR = nonproliferative diabetic retinopathy; NPS = nonperfusion square; PDR = proliferative diabetic retinopathy; PRP = panretinal photocoagulation; STTA = subTenon's injection of triamcinolone acetonide; VD = vessel density.

characteristics (Fig 3A–C). The heatmap analyses of the NPS counts in superficial and deep layers identified distinct spatial patterns: cases with minimal NPSs appeared on the right, whereas those with maximal NPSs were arranged in the lower left corner. Eyes in the superior region showed fewer superficial NPSs but more NPSs in the deep layer. Conversely, eyes with extensive NPSs in both layers were found in the inferior region. Eyes in the lower left corner were often accompanied with poor VA, thinner CST, and proliferative diabetic retinopathy (PDR; Fig 3D–F). Eyes with greater CST were randomly distributed (Fig 3F). Subset analyses were conducted on 220 eyes without any history of subTenon's injection of triamcinolone acetonide, anti-VEGF injections, or vitrectomy (Fig S4A, B, available at www.ophthalmologyscience.org), as well as on 195 eyes without DME (Fig S5A, B, available at www.ophthalmologyscience.org). The heatmaps of NPS amounts in both the superficial and deep layers showed similar trends.

Subsequent clustering divided 301 eyes into 5 groups named *Initial*, *Mild*, *Superficial*, *Moderate*, and *Severe* (Fig 6A). Statistical analysis showed that the *Superficial* and *Severe* groups had higher superficial NPS counts within the 2.5-mm circle compared with the *Initial* and *Mild* groups (Fig 6B). A stepwise increase in NPS counts was observed in the deep layer or both layers across the *Initial*, *Mild*, *Moderate*, and *Severe* groups (Fig 6C, D). Comparative analysis further highlighted differences in DR severity, CST, and notably, a significantly poorer logMAR VA within the *Severe* group (Table 2).

Additional analysis within each sector of the ETDRS grid revealed that the distinction between the *Superficial* and *Moderate* groups was evident in the superficial layer of the central sector, with no significant differences in the parafoveal sectors (Fig 7A, B). The superficial NPS counts were significantly higher in the *Severe* group across each quadrant of the parafoveal ring (Fig 7C–F). Statistical comparisons in the deep layer showed fewer NPS counts in the central sector for the *Initial* and *Mild* groups than in the *Superficial*, *Moderate*, and *Severe* groups, with no differences among the latter 3 (Fig 8A). The parafoveal sectors of the *Severe* group had more NPS counts than those of the *Superficial* and *Moderate* groups (Fig 8B–F). Deep NPS counts increased from the *Initial* to the *Severe* group in each quadrant of the parafoveal ring (Fig 8C–F). In the temporal quadrant, deep NPS counts were notably higher in eyes of the *Moderate* group compared with those of the *Superficial* group, with no significant differences noted in other quadrants (Fig 8C–F). The pseudocolored maps of NPS ratios confirmed these findings (Fig. 9). The NPS ratios were particularly elevated in the temporal quadrant for the *Mild*, *Superficial*, and *Moderate* groups, whereas the *Severe* group demonstrated higher NPS ratios predominantly in the parafoveal areas.

## Discussion

In this preliminary study, we introduced a novel severity scaling system for DMI on OCTA images, based on NPA distribution. Utilizing the UMAP algorithm, we projected multidimensional data into a comprehensible 2-dimensional space. The arrangement of DR cases on the UMAP space suggests a continuous severity scale for DMI and potential progression pathways for capillary nonperfusion within the macula. In contrast, subsequent clustering enabled us to divide DR cases into 5 groups and provided the discrete severity scale. The presence of the *Superficial* and *Moderate* groups in the intermediate stage suggests the existence of multiple progression pathways for DMI. A future longitudinal study is necessary to confirm these proposed severity scales and progression pathways.

This study provided a basis for classification by quantifying the amounts and distribution of NPSs. Previously, FA was utilized to assess the parameters of the FAZ; however, OCTA has demonstrated the associations between VA loss and capillary nonperfusion, particularly in the parafoveal and deep capillary plexuses.[14,16,17] Despite their clinical relevance, the diagnostic criteria and classification system for disease severity remains to be established. Our model proposes a solution by offering a means to categorize DMI severity, which could potentially guide targeted interventions.

We utilized NPSs as a novel metric to investigate the distribution and volume of macular capillary nonperfusion on en face OCTA images. This approach provides several

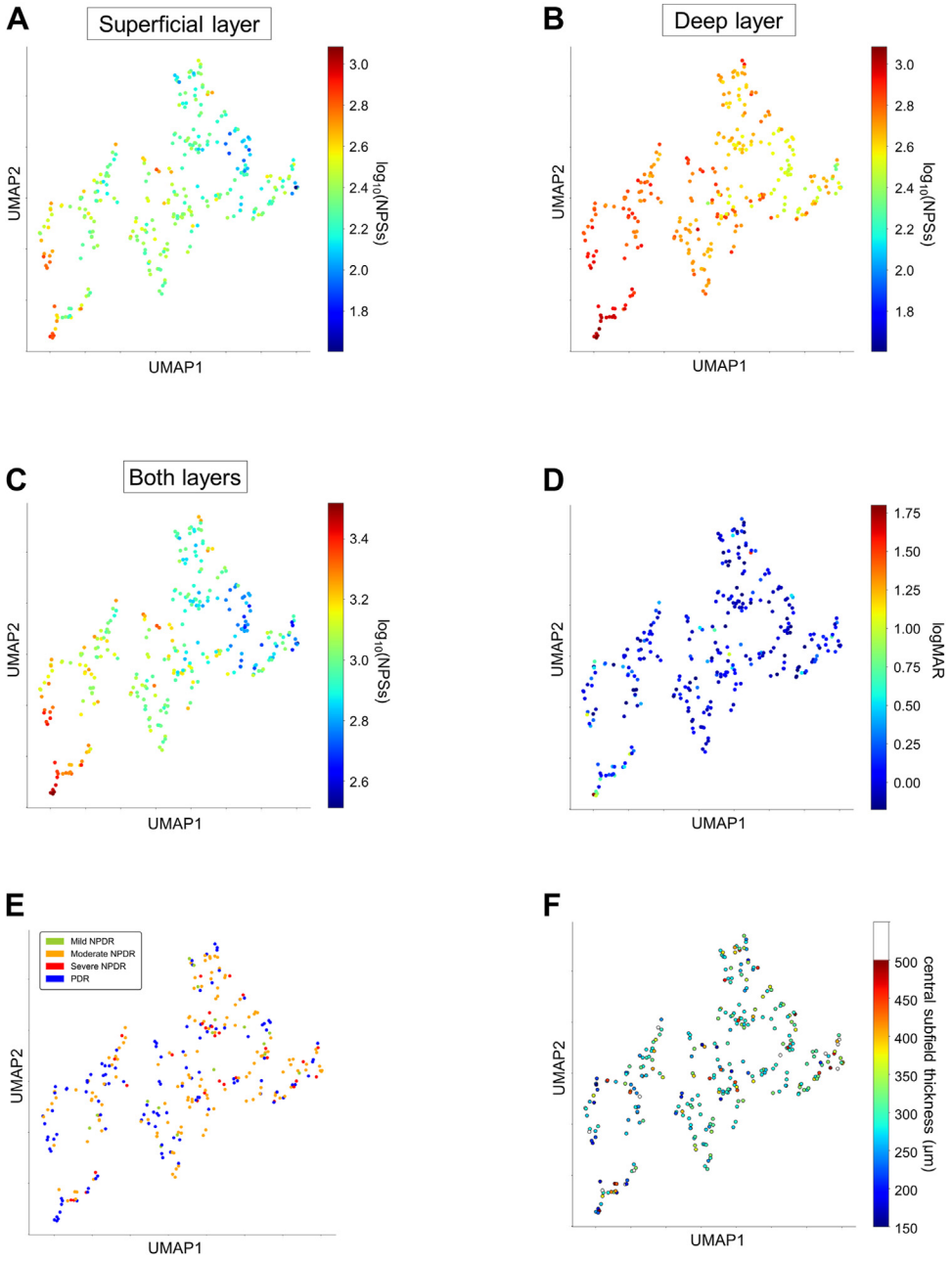


**Figure 3.** Visualization of each eye with diabetic retinopathy (DR) on a 2-dimensional pseudocolored map using the uniform manifold approximation and projection (UMAP) algorithm. Color coding indicates nonperfusion square counts in the superficial layer (**A**), in the deep layer (**B**), in both superficial and deep layers (**C**), logarithm of the minimum angle of resolution visual acuity (**D**), central subfield thickness (**E**), and DR severity grade (**F**). NPDR = nonproliferative diabetic retinopathy; PDR = proliferarive diabetic retinopathy.

advantages over traditional metrics like VD and FAZ size in previous publications.[3,4,14–16] Nonperfusion squares identified the precise locations of NPAs, compared with the VD.[26] By incorporating edge detection in our image processing, we aimed to minimize quantitative inaccuracies typically associated with poor image quality and suspended scattering particles in motion.[21,26] In cases with DME compared with those without, the correlation between VD and NPS was diminished. This reduction is attributed to suspended scattering particles in motion, which create a false impression of increased VD, thereby leading to its overestimation.[28]

Another point is the validity to evaluate NPAs on en face OCTA images despite the 3-dimensionality of retinal vasculature. We could not define capillary nonperfusion in the retinal parenchyma between capillary plexuses based on 3-dimensional voxels. However, the 2-dimensional nonperfusion areas observed in en face OCTA images

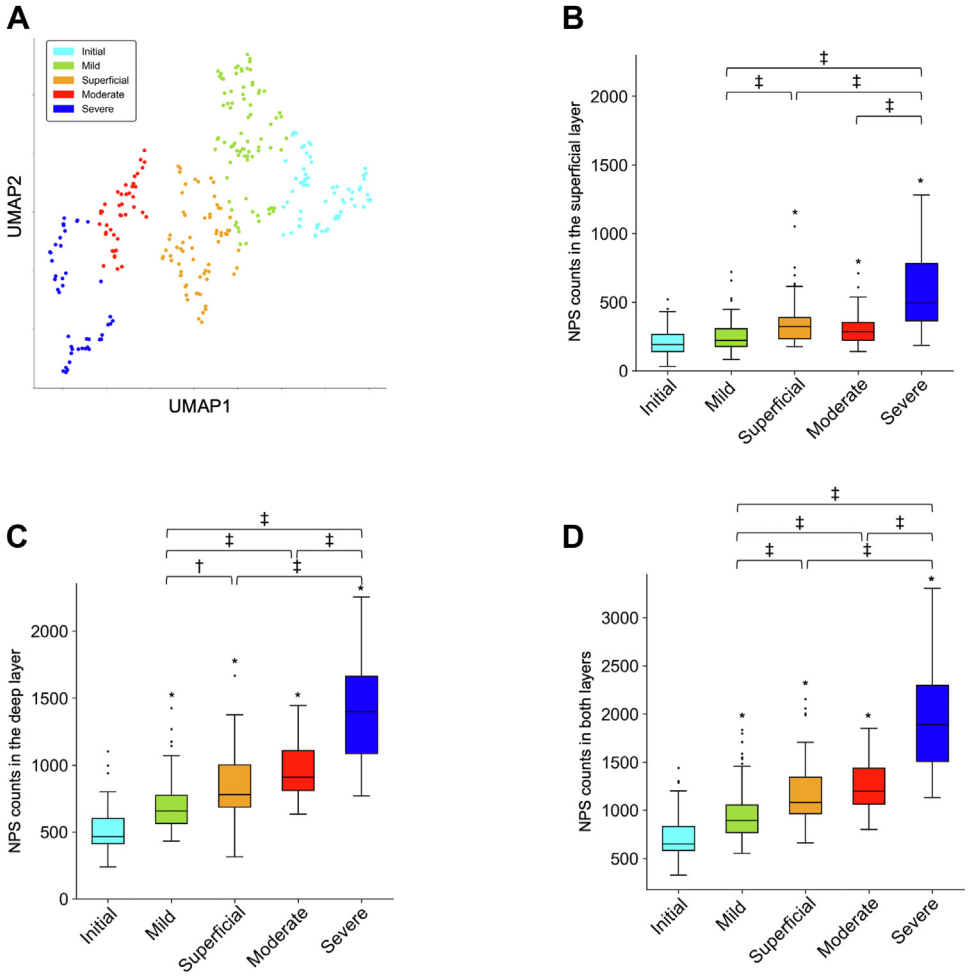


**Figure 6.** Nonperfusion areas in 5 groups which were determined by *k*-means clustering. **A,** Objective *k*-means clustering divides 301 eyes with diabetic retinopathy into 5 groups. Boxplots show nonperfusion square (NPS) counts across clusters for all 301 eyes: in the superficial layer (**B**), in the deep layer (**C**), and in both superficial and deep layers (**D**). *$P < 0.05$ vs. the Initial group; †$P < 0.05$; ‡$P < 0.01$. UMAP = uniform manifold approximation and projection.

correspond to ischemia in retinal columns. Additionally, the vascular structures and the types of surrounding cells, including neurons and glia, differ between the superficial and deep slabs, potentially affecting the development or progression of NPAs in each layer.[1] These pathophysiological considerations suggest that en face OCTA images are suitable for assessing capillary nonperfusion. Nonetheless, a 3-dimensional assessment of flow signals on OCTA images could provide more precise understanding of capillary nonperfusion, especially with adequate interpretation of the avascular parenchyma between vascular plexus layers.[8,29]

Visualization of DR cases on a 2-dimensional space might allow us to infer the progression profiles in each case, and the classification might engender the impacts of capillary nonperfusion on VA and neurodegeneration. Simply, we may specify the DMI severity grades from the *Initial*, *Mild*, *Moderate*, to *Severe*. Nonperfusion square counts gradually increased, although VA was poorer in eyes of the *Severe* group alone. Several pathophysiological mechanisms should be considered; different influences of transient and persistent obstruction on visual impairment, subsequent neurodegeneration, and the threshold for malnutrition.[5,30–35] Eyes with retinal thinning were more frequent in the *Severe* group, so neurodegeneration might contribute to the visual impairment at least in part.[36] The other point was the unique NPS profiles in the *Superficial* group; more NPSs in the central sector of the superficial layer and fewer NPSs in the temporal sector of the deep layer, compared with eyes with the *Moderate* group. It suggests that multiple mechanisms, e.g., inherent FAZ size and VD in the parafovea, neuroglial responses to hyperglycemia, and vascular permeability, regulate the branched progression of capillary nonperfusion until the intermediate stages of DMI.[37,38]

There are several limitations to this study. The inclusion and exclusion criteria were applied in this single-center study, which may result in selection bias. We utilized a specific SS-OCTA device and applied the specific image

Table 2. Clinical Parameters in Each Cluster

| Variables | Initial | Mild | Superficial | Moderate | Severe | P Value |
|---|---|---|---|---|---|---|
| Eyes | 64 | 81 | 67 | 44 | 45 | |
| Age (yrs) | 66 (53–70) | 66 (58–73) | 64 (53–72) | 68 (55–71) | 57 (47–66)† | 0.012 |
| Sex (male/female) | 41/23 | 55/26 | 39/28 | 25/19 | 36/9 | 0.114 |
| Hemoglobin A1c (%) | 7.3 (6.6–8.5) | 7.3 (6.7–8.5) | 7.2 (6.6–8.4) | 7.5 (6.8–8.5) | 7.9 (6.8–9.0) | 0.520 |
| Duration of diabetes (yrs) | 15 (8–22) | 15 (10–23) | 16 (10–22) | 18 (11–23) | 13 (9–20) | 0.744 |
| Systemic hypertension (present/absent) | 32/32 | 49/32 | 43/24 | 28/16 | 27/18 | 0.500 |
| Dyslipidemia (present/absent) | 29/35 | 28/53 | 27/40 | 21/23 | 19/26 | 0.603 |
| logMAR VA | −0.040 (−0.079 to 0.097) | 0.000 (−0.079 to 0.097) | 0.000 (−0.079 to 0.046) | 0.000 (−0.079 to 0.155) | 0.155 (0–0.398)*,†,‡,§ | <0.001 |
| Phakia/pseudophakia | 30/34 | 48/33 | 46/21 | 23/21 | 23/22 | 0.110 |
| International DR severity grade (eyes) | | | | | | |
| Mild NPDR | 4 | 7 | 4 | 3 | 0 | 0.045 |
| Moderate NPDR | 34 | 38 | 32 | 20 | 15 | |
| Severe NPDR | 8 | 13 | 2 | 4 | 4 | |
| PDR | 18 | 23 | 29 | 17 | 26 | |
| Diabetic macular edema (present/absent) | 33/31 | 28/53 | 16/51 | 14/30 | 15/30 | 0.021 |
| Central subfield thickness (μm) | 313 (289–379) | 289 (272–342) | 285 (267–306)* | 288 (263–324) | 267 (222–376) | <0.001 |
| FAZ size in the superficial layer ($mm^2$) | 0.29 (0.24–0.33) | 0.36 (0.29–0.45)* | 0.49 (0.42–0.63)*,† | 0.40 (0.34–0.52)*,‡ | 0.75 (0.56–0.99)*,†,‡,§ | <0.001 |
| VD in the superficial layer (%) | 36.7 (32.0–41.9) | 37.9 (33.6–42.6) | 35.5 (31.3–39.6) | 36.9 (33.5–40.1) | 30.9 (23.8–37.5)*,†,‡,§ | <0.001 |
| VD in the deep layer (%) | 22.9 (16.0–26.2) | 21.5 (15.2–26.2) | 18.0 (14.5–23.0)* | 17.0 (14.7–21.2) | 13.7 (8.59–18.0)*,†,‡,§ | <0.001 |
| Prior PRP (present/absent) | 20/44 | 26/55 | 29/38 | 22/22 | 27/18*,† | 0.009 |
| Prior STTA (present/absent) | 6/58 | 7/74 | 3/64 | 5/39 | 4/41 | 0.744 |
| Prior anti-VEGF injection (present/absent) | 11/53 | 15/66 | 2/65 | 5/39 | 6/39 | 0.055 |
| Prior vitrectomy (present/absent) | 9/55 | 6/75 | 6/61 | 4/40 | 10/35 | 0.115 |

DR = diabetic retinopathy; logMAR VA = logarithm of the minimum angle of resolution visual acuity; NPDR = nonproliferative diabetic retinopathy; NPS = nonperfusion square; PDR = proliferative diabetic retinopathy; FAZ = foveal avascular zone; VD = vessel density; PRP = panretinal photocoagulation; STTA = subTenon's injection of triamcinolone acetonide.
*$P < 0.05$ vs. Initial.
†$P < 0.01$ vs. Mild.
‡$P < 0.05$ vs. Superficial.
§$P < 0.05$ vs. Moderate.

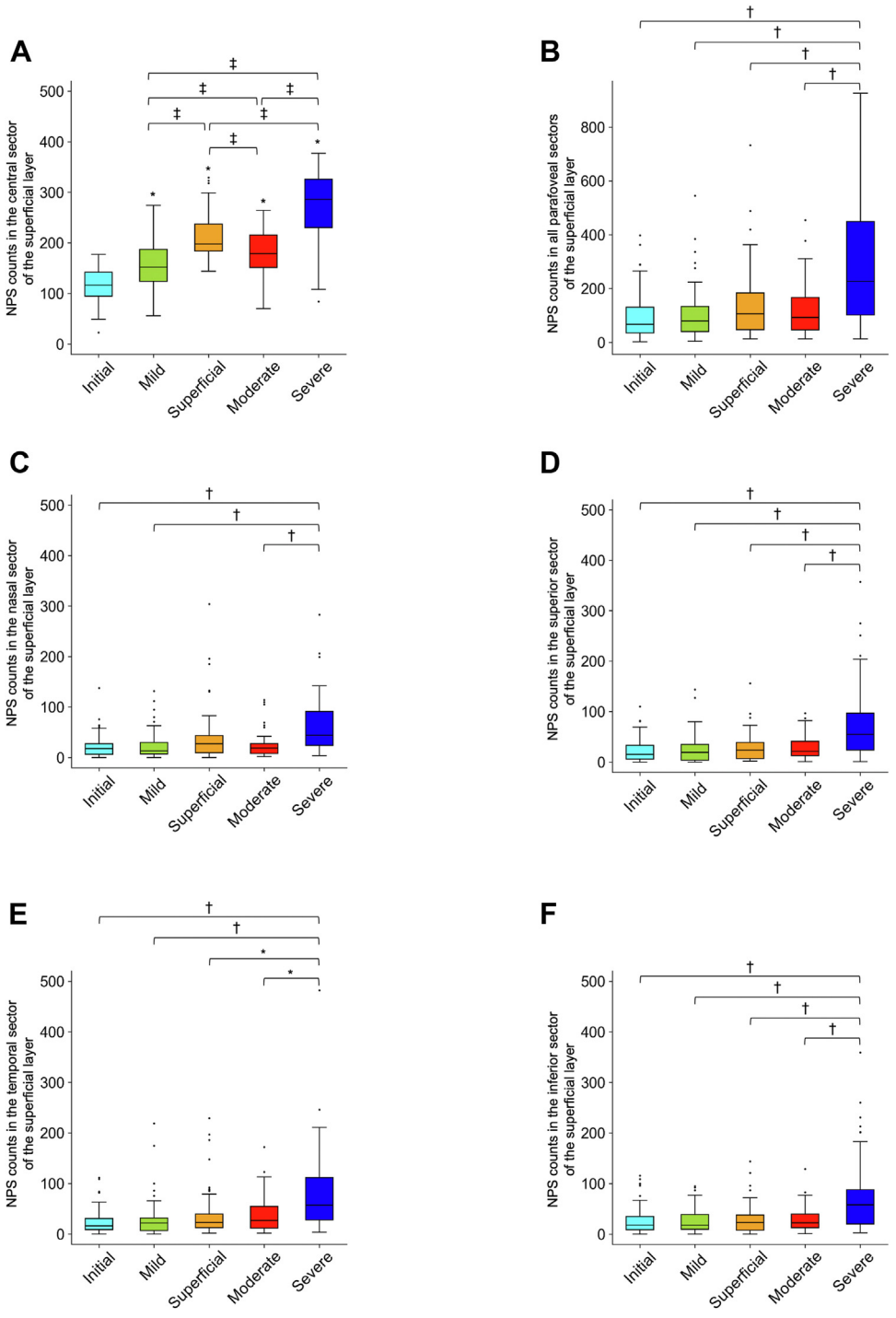


**Figure 7.** The nonperfusion square (NPS) amounts in each sector in the superficial layer. Boxplots show NPS counts in the superficial layer across clusters for all 301 eyes with diabetic retinopathy: in the central sector (**A**), in all parafoveal sectors (**B**), in the nasal (**C**), superior (**D**), temporal (**E**), and inferior (**F**) sectors of the parafoveal area. *$P < 0.05$; †$P < 0.01$.

processing.[39,40] In particular, segmentation errors might have led to incorrect quantification in eyes with DME. To address this, we selected objective methods to segment the superficial and deep layers, excluding cases with severe segmentation errors. A recent publication highlighted the usefulness of subjective and manual correction of segmentation in eyes with DME.[41] Future multicenter studies using different image acquisition

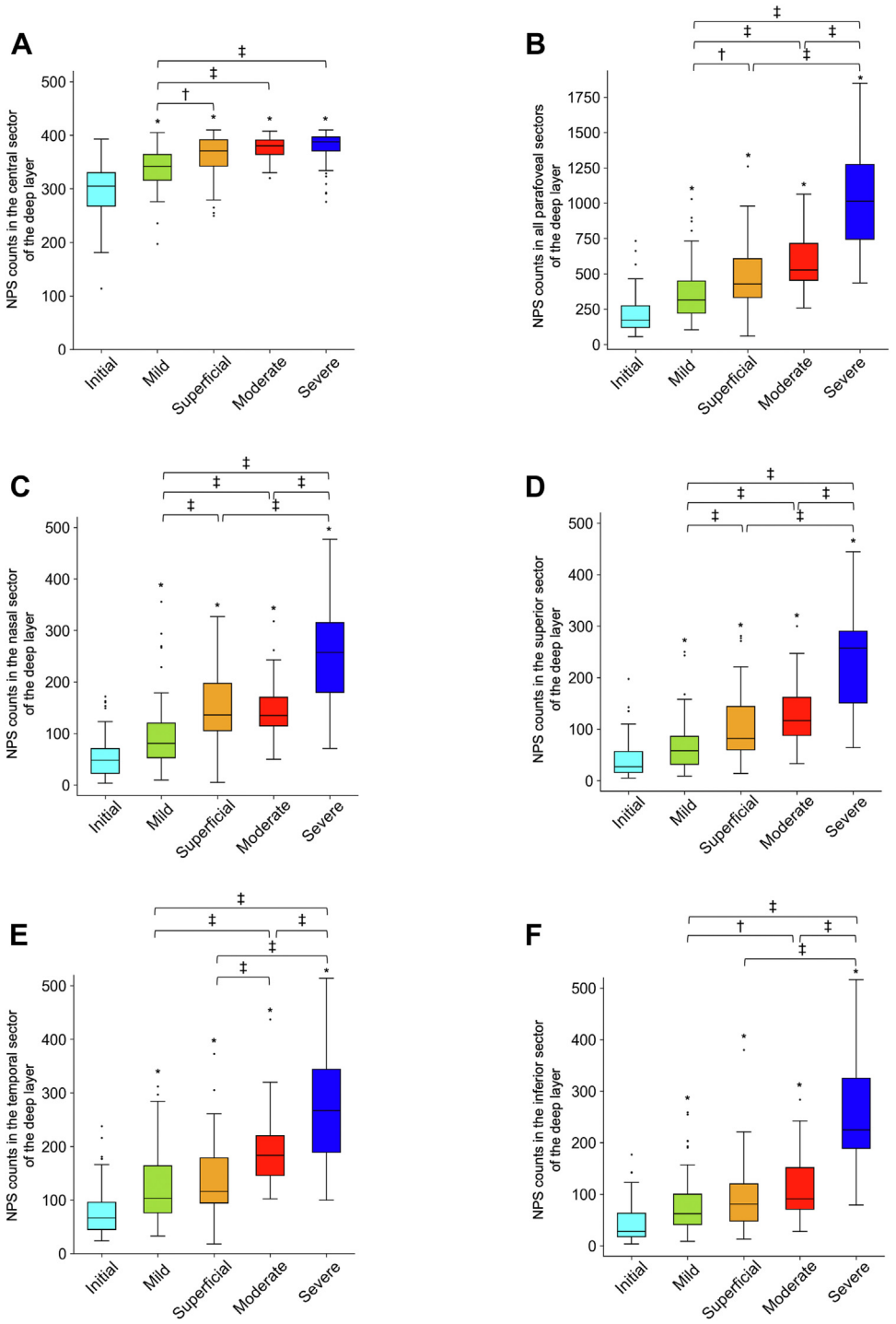


**Figure 8.** The nonperfusion square (NPS) amounts in each sector in the deep layer. Boxplots show NPS counts in the deep layer across clusters for all 301 eyes with diabetic retinopathy: in the central sector (**A**), in all parafoveal sectors (**B**), in the nasal (**C**), superior (**D**), temporal (**E**), and inferior (**F**) sectors of the parafoveal area. *$P < 0.05$ versus the Initial group; †$P < 0.05$; ‡$P < 0.01$.

devices and other algorithms to detect vessels on OCTA images should show the generalizability.[42] Although UMAP and subsequent *k*-means clustering were utilized in this study, other algorithms for dimensionality reduction and clustering may lead to other feature extraction or unsupervised classifications.[43–45] We presented a severity scale of DMI based on the NPA distribution alone, and future study should show the association between NPA distribution and retinal functional examinations other than VA.

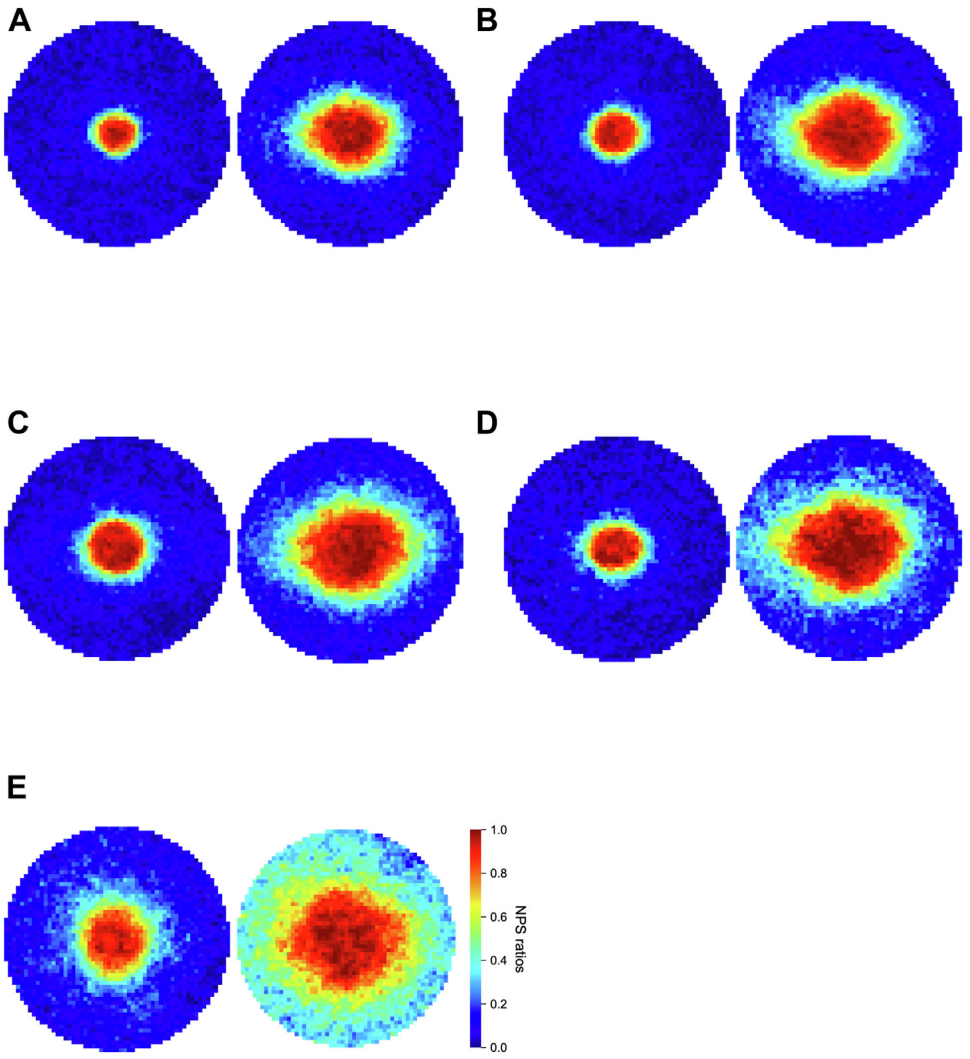


**Figure 9.** The heatmaps show the nonperfusion square (NPS) ratios in each square of each cluster in the superficial (left) and deep (right) layers. **A,** The NPS ratios in the *Initial* group display minimal nonperfusion areas (NPAs) in both superficial and deep layers. **B,** The ratios in the *Mild* group shows a mild increase in NPAs in the deep layer. **C,** The heatmap in the *Superficial* group is characterized by larger NPAs in the superficial layer of the central sector. **D,** In the *Moderate* group, the NPAs extended to the temporal subfield in the deep layer. **E,** The NPS ratios in the *Severe* group are higher in both layers. The nasal quadrant is shown on the right-hand side.

In conclusion, we proposed a novel severity scale for diabetic capillary nonperfusion in the macula on OCTA images. This preliminary study would contribute to the further investigation to establish the diagnostic and staging criteria for DMI.

## Footnotes and Disclosures

Originally received: May 20, 2024.
Final revision: August 6, 2024.
Accepted: August 9, 2024.
Available online: September 7, 2024. Manuscript no. XOPS-D-24-00156R1.

Department of Ophthalmology and Visual Sciences, Kyoto University Graduate School of Medicine, Kyoto, Japan.

Disclosures:

All authors have completed and submitted the ICMJE disclosures form.

The authors have no proprietary or commercial interest in any materials discussed in this article.

This study was funded by a Grant-in-Aid for Scientific Research of the Japan Society for the Promotion of Science (Grant Number: 20K09788 and 23K09004). The funding organization had no role in the design or conduct of this research.

HUMAN SUBJECTS: Human subjects were included in this study. This study was conducted under the approval of the Kyoto University Graduate School and Faculty of Medicine Ethics Committee and in adherence to the

tenets of the Declaration of Helsinki. All participants provided written informed consent before inclusion in the study.

No animal subjects were used in this study.

Author Contributions:

Conception and design: Yoshida, Murakami

Data collection: Yoshida, Murakami, Nishikawa, Ishihara, Mori, Tsujikawa

Analysis and interpretation: Yoshida, Murakami, Tsujikawa

Obtained funding: Murakami

Overall responsibility: Yoshida, Murakami

Abbreviations and Acronyms:
**CST** = central subfield thickness; **DME** = diabetic macular edema; **DMI** = diabetic macular ischemia; **DR** = diabetic retinopathy; **FA** = fluorescein angiography; **FAZ** = foveal avascular zone; **logMAR** = logarithm of the minimum angle of resolution; **NPAs** = nonperfusion areas; **NPDR** = nonproliferative diabetic retinopathy; **NPSs** = nonperfusion squares; **OCTA** = OCT angiography; **PDR** = proliferative diabetic retinopathy; **SS** = swept-source; **UMAP** = uniform manifold approximation and projection; **VA** = visual acuity; **VD** = vessel density.

Keywords:
Diabetic macular ischemia, Diabetic retinopathy, Nonperfusion areas, Semiautomatic quantification, Uniform manifold approximation and projection.

Correspondence:
Tomoaki Murakami, MD, PhD, 54 Shougoin Kawahara-cho, Sakyo-ku, Kyoto 606-8507, Japan. E-mail: mutomo@kuhp.kyoto-u.ac.jp.

## References

1. Antonetti DA, Klein R, Gardner TW. Diabetic retinopathy. *N Engl J Med*. 2012;366:1227−1239.
2. Sim DA, Keane PA, Zarranz-Ventura J, et al. The effects of macular ischemia on visual acuity in diabetic retinopathy. *Invest Ophthalmol Vis Sci*. 2013;54:2353−2360.
3. Balaratnasingam C, Inoue M, Ahn S, et al. Visual acuity is correlated with the area of the foveal avascular zone in diabetic retinopathy and retinal vein occlusion. *Ophthalmology*. 2016;123:2352−2367.
4. Samara WA, Shahlaee A, Adam MK, et al. Quantification of diabetic macular ischemia using optical coherence tomography angiography and its relationship with visual acuity. *Ophthalmology*. 2017;124:235−244.
5. Tsai WS, Thottarath S, Gurudas S, et al. Characterization of the structural and functional alteration in eyes with diabetic macular ischemia. *Ophthalmol Retina*. 2023;7:142−152.
6. Tsai ASH, Gan ATL, Ting DSW, et al. Diabetic macular ischemia: correlation of retinal vasculature changes by optical coherence tomography angiography and functional deficit. *Retina*. 2020;40:2184−2190.
7. Cheung CMG, Fawzi A, Teo KYC, et al. Diabetic macular ischaemia- a new therapeutic target? *Prog Retin Eye Res*. 2022;89:101033.
8. Waheed NK, Rosen RB, Jia Y, et al. Optical coherence tomography angiography in diabetic retinopathy. *Prog Retin Eye Res*. 2023;97:101206.
9. Snodderly DM, Weinhaus RS, Choi JC. Neural-vascular relationships in central retina of macaque monkeys (Macaca fascicularis). *J Neurosci*. 1992;12:1169−1193.
10. Jia Y, Tan O, Tokayer J, et al. Split-spectrum amplitude-decorrelation angiography with optical coherence tomography. *Opt Express*. 2012;20:4710−4725.
11. Choi W, Moult EM, Waheed NK, et al. Ultrahigh-speed, swept-source optical coherence tomography angiography in nonexudative age-related macular degeneration with geographic atrophy. *Ophthalmology*. 2015;122:2532−2544.
12. Early Treatment Diabetic Retinopathy Study Research Group. Classification of diabetic retinopathy from fluorescein angiograms. ETDRS report number 11. *Ophthalmology*. 1991;98:807−822.
13. Spaide RF, Klancnik JM, Cooney MJ. Retinal vascular layers imaged by fluorescein angiography and optical coherence tomography angiography. *JAMA Ophthalmol*. 2015;133:45−50.
14. Yang D, Tang Z, Ran A, et al. Assessment of parafoveal diabetic macular ischemia on optical coherence tomography angiography images to predict diabetic retinal disease progression and visual acuity deterioration. *JAMA Ophthalmol*. 2023;141:641−649.
15. Durbin MK, An L, Shemonski ND, et al. Quantification of retinal microvascular density in optical coherence tomographic angiography images in diabetic retinopathy. *JAMA Ophthalmol*. 2017;135:370−376.
16. Lee J, Moon BG, Cho AR, Yoon YH. Optical coherence tomography angiography of DME and its association with anti-VEGF treatment response. *Ophthalmology*. 2016;123:2368−2375.
17. Terada N, Murakami T, Ishihara K, et al. Clinical relevance of parafoveal intercapillary spaces and foveal avascular zone in diabetic retinopathy without macular edema. *Invest Ophthalmol Vis Sci*. 2022;63:4.
18. Becht E, McInnes L, Healy J, et al. Dimensionality reduction for visualizing single-cell data using UMAP. *Nat Biotechnol*. 2019;37:38−44.
19. McInnes L, Healy J, Melville J. Uniform manifold approximation and projection for dimension reduction. Preprint. Posted online February 8, 2018. *arXiv*. abs/1802.03426. https://arxiv.org/abs/1802.03426
20. Wu Y, Egan C, Olvera-Barrios A, et al. Developing a continuous severity scale for macular telangiectasia Type 2 using deep learning and implications for disease grading. *Ophthalmology*. 2024;131:219−226.
21. Yoshida M, Murakami T, Kawai K, et al. Inference of capillary nonperfusion progression on widefield OCT angiography in diabetic retinopathy. *Invest Ophthalmol Vis Sci*. 2023;64:24.
22. Wilkinson CP, Ferris FL, Klein RE, et al. Proposed international clinical diabetic retinopathy and diabetic macular edema disease severity scales. *Ophthalmology*. 2003;110:1677−1682.
23. Chalam KV, Bressler SB, Edwards AR, et al. Retinal thickness in people with diabetes and minimal or no diabetic retinopathy: Heidelberg spectralis optical coherence tomography. *Invest Ophthalmol Vis Sci*. 2012;53:8154−8161.
24. Terada N, Murakami T, Ishihara K, et al. Quantification of dilated deep capillaries in diabetic retinopathy on optical coherence tomography angiography. *Sci Rep*. 2023;13:17884.
25. Canny J. A computational approach to edge detection. *IEEE Trans Pattern Anal Mach Intell*. 1986;8:679−698.
26. Kawai K, Murakami T, Mori Y, et al. Clinically significant nonperfusion areas on widefield OCT angiography in diabetic retinopathy. *Ophthalmol Sci*. 2023;3:100241.

27. Kawai K, Murakami T, Sakaguchi S, et al. Peripheral chorioretinal imaging through a front prism on optical coherence tomography angiography. *Transl Vis Sci Technol*. 2021;10:36.
28. Maltsev DS, Kulikov AN, Kazak AA, et al. Suspended scattering particles in motion may influence optical coherence tomography angiography vessel density metrics in eyes with diabetic macular edema. *Retina*. 2021;41:1259–1264.
29. Wang B, Camino A, Pi S, et al. Three-dimensional structural and angiographic evaluation of foveal ischemia in diabetic retinopathy: method and validation. *Biomed Opt Express*. 2019;10:3522.
30. Stitt AW, Curtis TM, Chen M, et al. The progress in understanding and treatment of diabetic retinopathy. *Prog Retin Eye Res*. 2016;51:156–186.
31. Miyamoto K, Khosrof S, Bursell S, et al. Prevention of Leukostasis and Vascular Leakage in Streptozotocin-Induced Diabetic Retinopathy via Intercellular Adhesion Molecule-1 Inhibition. *Proc Natl Acad Sci U S A*. 1999;96:10836–10841.
32. Sun JK, Lin MM, Lammer J, et al. Disorganization of the retinal inner layers as a predictor of visual acuity in eyes with center-involved diabetic macular edema. *JAMA Ophthalmol*. 2014;132:1309–1316.
33. Dodo Y, Murakami T, Uji A, et al. Disorganized retinal lamellar structures in nonperfused areas of diabetic retinopathy. *Invest Ophthalmol Vis Sci*. 2015;56:2012–2020.
34. Dodo Y, Murakami T, Suzuma K, et al. Diabetic neuroglial changes in the superficial and deep nonperfused areas on optical coherence tomography angiography. *Invest Ophthalmol Vis Sci*. 2017;58:5870–5879.
35. Scarinci F, Jampol LM, Linsenmeier RA, Fawzi AA. Association of diabetic macular nonperfusion with outer retinal disruption on optical coherence tomography. *JAMA Ophthalmol*. 2015;133:1036–1044.
36. Sim DA, Keane PA, Fung S, et al. Quantitative analysis of diabetic macular ischemia using optical coherence tomography. *Invest Ophthalmol Vis Sci*. 2014;55:417–423.
37. Bowl W, Bowl M, Schweinfurth S, et al. OCT angiography in young children with a history of retinopathy of prematurity. *Ophthalmol Retina*. 2018;2:972–978.
38. Barber AJ, Lieth E, Khin SA, et al. Neural apoptosis in the retina during experimental and human diabetes. Early onset and effect of insulin. *J Clin Invest*. 1998;102:783–791.
39. Spaide RF, Fujimoto JG, Waheed NK. Image artifacts in optical coherence tomography. *Retina*. 2015;35:2163–2180.
40. Ghasemi Falavarjani K, Al-Sheikh M, Akil H, Sadda SR. Image artefacts in swept-source optical coherence tomography angiography. *Br J Ophthalmol*. 2017;101:564–568.
41. Ghasemi Falavarjani K, Habibi A, Anvari P, et al. Effect of segmentation error correction on optical coherence tomography angiography measurements in healthy subjects and diabetic macular oedema. *Br J Ophthalmol*. 2020;104:162–166.
42. Spaide RF, Fujimoto JG, Waheed NK, et al. Optical coherence tomography angiography. *Prog Retin Eye Res*. 2018;64:1–55.
43. Hotelling H. Analysis of a complex of statistical variables into principal components. *J Edu Psychol*. 1933;24:417–441.
44. Kruskal JB. Multidimensional scaling by optimizing goodness of fit to a nonmetric hypothesis. *Psychometrika*. 1964;29:1–27.
45. Van Der Maaten L, Hinton G. Visualizing data using T-SNE. *J Mach Learn Res*. 2008;9:2579–2605.